Proportional-derivative sliding mode control for mobile lifting and transferring robot

Trong Hieu Do[1*], Thanh Phuong Tran[1], Minh Duc Duong[1] and Nga Nguyen Thi Thanh[2]

[1]*School of Electrical and Electronic Engineering, Hanoi University of Science and Technology*
[2]*School of Information and Communication Technology, Hanoi University of Science and Technology*
[*]*Corresponding author E-mail:hieu.dotrong@hust.edu.vn*
DOI: https://doi.org/10.64032/mca.v30i2.424

Abstract

The task of lifting and transferring mobility-impaired patients demands stringent standards for safety and stability. However, most current assistive devices operate manually and lack an active sway suppression mechanism, easily leading to payload oscillations and inducing psychological anxiety in patients. To address this issue, this paper proposes a Proportional-Derivative Sliding Mode Control (PD-SMC) approach specifically designed to suppress payload oscillations and ensure autonomous trajectory tracking for a mobile patient lifting and transferring system. The investigated system consists of a differential-drive mobile robot combined with a load suspension mechanism. This proposed control method simplifies the structure of the traditional sliding mode controller while maintaining superior disturbance rejection against uncertainties such as variations in patient mass and exogenous disturbances. The results demonstrate that the PD-SMC controller generates smooth control signals, forcing the state trajectories to converge rapidly, thereby enabling the system to accurately track the moving trajectory and completely suppress payload oscillations. This proposed approach not only improves operational efficiency but also ensures maximum safety and provides a smooth experience for the patient.

Keywords: *Proportional-Derivative Sliding Mode Control; Robust; Mobile Lifting and Transferring; Model-Free.*

Abbreviations

PD-SMC	Proportional-Derivative Sliding Mode Control
ADRC	Active Disturbance Rejection Control
IS	Input Shaping
SMC	Sliding Mode Control

1. Introduction

In recent years, core technologies such as robotics, automation, intelligent control, and artificial intelligence have driven profound transformations across various sectors, including healthcare and patient care. The need to reduce the workload for healthcare professionals, improve service quality, and ensure patient safety has become increasingly urgent, particularly in frontline hospitals or high-density medical facilities. This has sparked growing interest in patient lifting and transfer devices-systems that play a vital role in rehabilitation care and intra-hospital transportation.

The task of moving mobility-impaired patients has long been a major challenge in clinical environments, posing potential injury risks to caregivers and causing psychological anxiety for patients [1]. To address this issue, various patient lifting and transfer devices have been extensively researched and commercialized. In practice, these systems have undergone numerous developmental iterations, ranging from manual lifting mechanisms [2] and hydraulic lifting platforms to ceiling-mounted [3] or wall-mounted suspension systems [4], and more recently, motorized electric lifters [5] [6]. Despite their high durability and low cost, a fundamental technical limitation persists across almost all current versions: they rarely integrate an active dynamic control mechanism, relying heavily instead on the direct manual operation of healthcare staff.

The absence of automated controllers renders current commercial patient lifters inflexible and inefficient, as their operation depends almost entirely on the user's manual handling [7]. Without a motion control mechanism, these systems often lack the ability to dampen payload sway, are prone to instability during movement or sudden stops, and cannot adapt to variations in patient mass or posture. When the device starts, brakes abruptly, or changes direction, the patient's body mass suspended on the lifting mechanism generates uncontrollable lateral and longitudinal swinging oscillations. This inability to suppress sway not only reduces operational efficiency and limits movement speed but also poses safety hazards, collision risks, and induces feelings of instability and fear in patients.

To address these limitations, this study introduces a mobile patient lifting system with integrated anti-swing control. The design features a differential-drive mobile robot paired with a patient hoisting mechanism. Its key innovation over traditional systems is autonomous navigation along predefined trajectories without human input. Instead of manual control, the controller automatically computes and adjusts actuator velocities, enabling smooth trajectory tracking while substantially reducing sway in the suspension cables. This maximizes safety, delivers a comfortable patient experience, and elevates a standard lifter into an intelligent, autonomous medical robot.

From a control theory perspective, stabilizing this highly nonlinear underactuated system poses major challenges, exacerbated by uncertainties like varying patient weights and

Received: 9 March 2026; Revised: 2 April 2026; Accepted: 14 April 2026.

Figure 1: Mobile patient lifting and transferring system

external disturbances. Classical PID methods, though tested, have proven sluggish and unstable under disturbances [8]. Recent alternatives-such as Sliding Mode Control (SMC) [9] or Active Disturbance Rejection Control (ADRC) [10] [11] paired with Input Shaping (IS) [12] [13]-offer better disturbance rejection and stability. However, SMC implementations struggle with issues like chattering, high switching frequencies, reaching phases, sliding surface selection, and ensuring sliding mode existence [14]. Meanwhile, ADRC-IS improves disturbance compensation but is hampered by signal delays that slow responses and degrade performance [15]. To fully address this complex nonlinear control problem, this paper proposes the application of the Proportional-Derivative Sliding Mode Control (PD-SMC) strategy [16] [17] to a novel autonomous patient lifting and transferring system. Traditional SMC offers robust disturbance rejection, but its control laws become cumbersome and impractical for high-order systems. By adapting the PD-SMC framework to this specific model, the controller structure is simplified, effectively overcoming these challenges. In this system, the adopted PD-SMC generates the effort to drive state trajectories onto the sliding surface and toward equilibrium. The PD component's linear action prevents abrupt signal fluctuations, rapidly suppressing payload sway and maximizing patient safety during lifting and transfer.

2. Mathematical model

2.1 System description

In the study of patient lifting and transferring devices, the actual system model can be highly complex due to the involvement of various mechanical components, control systems, and environmental factors that affect operation. To simplify the analysis, an equivalent model can be proposed that retains the essential characteristics of the system while reducing unnecessary complexity. Specifically, if the real system includes a lifting mechanism with multiple joints and complex sensors, a simplified model (Figure 1) can be constructed. This model consists of a differential drive mobile robot equipped with a support frame and a suspended cable, with two oscillation angles: θ_1 in the horizontal direction and θ_2 in the longitudinal direction, aligned with the robot's translational motion.

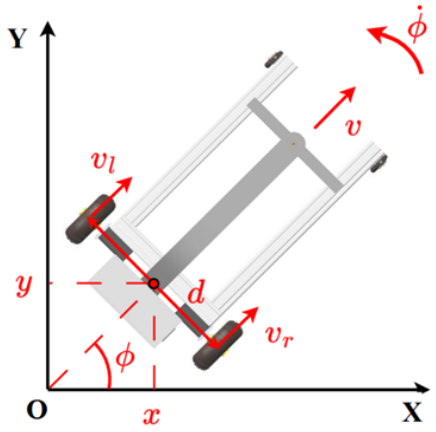

Figure 2: Description of system's parameters in Oxy coordinate plane

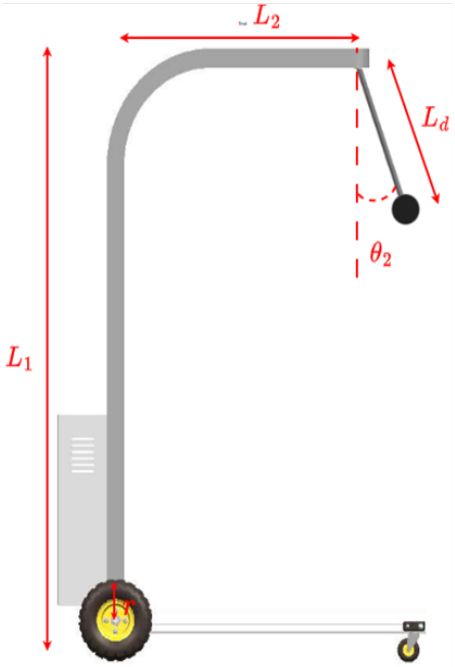

Figure 3: Description of system's parameters in Oxz coordinate plane

The system parameters, as described in Figure 2-4, include:
τ_r, τ_l: torques applied to the right and left wheels, respectively, which generate the driving force for the mobile base motion.
θ_r, θ_l: angular positions of the right and left wheels, representing the rotational displacement of each wheel over time.
ϕ: heading angle of the mobile base, describing its orientation with respect to the global reference frame.
θ_1, θ_2: swing angles of the suspended cable, indicating the deviation of the payload from the vertical equilibrium position in two orthogonal directions.
L_1: height of the suspension frame, representing the vertical distance from the mobile base to the suspension mechanism.
L_2: distance from the wheel center to the suspension point, defining the geometric offset between the driving wheels and the lifting mechanism.

r: wheel radius.
d: distance between the two wheels, also known as the track width, affecting the turning kinematics of the mobile platform.
m_p: mass of the mobile platform, representing the total mass of the robot body excluding wheels and payload.
I_p: moment of inertia of the platform about its vertical axis, influencing the rotational dynamics during turning.
I_w: moment of inertia of each wheel about its rotation axis, affecting wheel acceleration and torque response.
m_w: mass of each wheel, contributing to the overall system inertia and dynamics.
g: gravitational acceleration.
m_d: combined mass of the lifting cable and the load, treated as a lumped mass at the end of the suspension.
L_d: length of the suspended cable, determining the natural frequency and swing dynamics of the payload.
I_d: moment of inertia of the payload about the vehicle's rotational motion, representing its resistance to rotational acceleration.

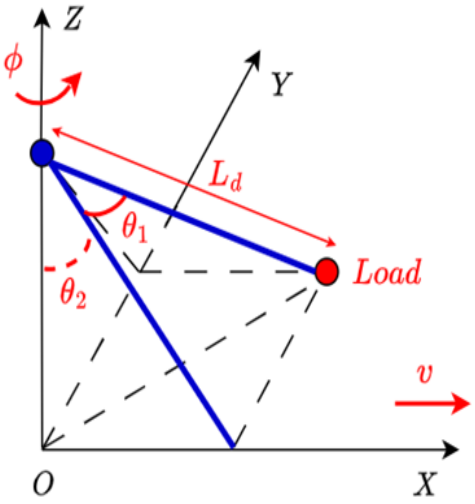

Figure 4: Load position description using two swing angles in Oxyz coordinate

2.2 System's mathematical model

The geometric and kinematic parameters are illustrated in Figure 2. The position and center of mass of the mobile robot are given (x,y), resulting in corresponding velocities $\dot{x}$ and $\dot{y}$. The positions of the centers of mass of the right wheel (x_r, y_r) and the left wheel (x_l, y_l) are given by:

$$x_r = x + \frac{d}{2}\sin\phi, \quad y_r = y - \frac{d}{2}\cos\phi \tag{1}$$

$$x_l = x - \frac{d}{2}\sin\phi, \quad y_l = y + \frac{d}{2}\cos\phi \tag{2}$$

The position (x_d, y_d, z_d) of the centers of mass for the transfer object (patient) is given by:

$$x_d = x + L_2\cos\phi + L_d\cos\theta_1\sin\theta_2\cos\phi - L_d\sin\theta_1\sin\phi \tag{3}$$

$$y_d = y + L_2\sin\phi + L_d\cos\theta_1\sin\theta_2\sin\phi + L_d\sin\theta_1\cos\phi \tag{4}$$

$$z_d = L_1 - L_d\cos\theta_1\cos\theta_2 \tag{5}$$

The kinetic energy of the system is determined by the sum of the kinetic energy of the load (K_p), the robot (K_d), and the motion of two wheels (K_r and K_l):

$$K = K_p + K_d + K_r + K_l \tag{6}$$

The individual kinetic energy components are calculated as follows [18]:

$$K_p = \frac{1}{2}m_p(\dot{x}^2 + \dot{y}^2) + \frac{1}{2}I_p\dot{\phi}^2 \tag{7}$$

$$K_r = \frac{1}{2}m_w(\dot{x}_r^2 + \dot{y}_r^2) + \frac{1}{2}I_{zw}\dot{\phi}^2 + \frac{1}{2}I_{yw}\dot{\theta}_r^2 \tag{8}$$

$$K_l = \frac{1}{2}m_w(\dot{x}_l^2 + \dot{y}_l^2) + \frac{1}{2}I_{zw}\dot{\phi}^2 + \frac{1}{2}I_{yw}\dot{\theta}_l^2 \tag{9}$$

$$K_d = \frac{1}{2}m_d(\dot{x}_d^2 + \dot{y}_d^2 + \dot{z}_d^2) + \frac{1}{2}I_d\dot{\phi}^2 \tag{10}$$

The potential energy of the system is determined as:

$$P = m_d g(L_1 - L_d\cos\theta_1\cos\theta_2) \tag{11}$$

And the nonholonomic constraints are given as follows [19]:

$$\dot{x} = \frac{r}{2}(\dot{\theta}_r + \dot{\theta}_l)\cos\phi \tag{12}$$

$$\dot{y} = \frac{r}{2}(\dot{\theta}_r + \dot{\theta}_l)\sin\phi \tag{13}$$

$$\dot{\phi} = \frac{r}{d}(\dot{\theta}_r - \dot{\theta}_l) \tag{14}$$

The Euler-Lagrange dynamic equations are described as:

$$\frac{d}{dt}\frac{\partial L}{\partial \dot{\theta}_i} - \frac{\partial L}{\partial \theta_i} = \tau_i \tag{15}$$

where $L = K - P$. From the Euler-Lagrange equation, the dynamical model of the system is derived in the general form as:

$$M(q)\ddot{q} + C(q,\dot{q})\dot{q} + G(q) = \tau \tag{16}$$

The detailed description of $M(q)\ddot{q}, C(q,\dot{q})\dot{q}, G(q)$ is shown in Appendix A. This model is used to design the system's controller.

3. Design of PD-SMC controller

3.1 Controller design

From the dynamic model established above, we can rewrite it in the form:

$$M_{11}\ddot{q}_1 + M_{12}\ddot{q}_2 + C_{11}\dot{q}_1 + C_{12}\dot{q}_2 = u \tag{17}$$

$$M_{21}\ddot{q}_1 + M_{22}\ddot{q}_2 + C_{21}\dot{q}_1 + C_{22}\dot{q}_2 + G_2 = 0 \tag{18}$$

where $q_1 = [\theta_r \quad \theta_l]^T, q_2 = [\theta_1 \quad \theta_2]^T$ and $u = [\tau_r \quad \tau_l]$. In addition,

$$M_{11} = \begin{bmatrix} m_{11} & m_{12} \\ m_{21} & m_{22} \end{bmatrix}, M_{12} = \begin{bmatrix} m_{13} & m_{14} \\ m_{23} & m_{24} \end{bmatrix}, M_{21} = \begin{bmatrix} m_{31} & m_{32} \\ m_{41} & m_{42} \end{bmatrix}$$

$$M_{22} = \begin{bmatrix} m_{33} & m_{34} \\ m_{43} & m_{44} \end{bmatrix}, C_{11} = \begin{bmatrix} c_{11} & c_{12} \\ c_{21} & c_{22} \end{bmatrix}, C_{12} = \begin{bmatrix} c_{13} & c_{14} \\ c_{23} & c_{24} \end{bmatrix}$$

$$C_{21} = \begin{bmatrix} c_{31} & c_{32} \\ c_{41} & c_{42} \end{bmatrix}, C_{22} = \begin{bmatrix} c_{33} & c_{34} \\ c_{43} & c_{44} \end{bmatrix}, G_2 = \begin{bmatrix} g_{31} \\ g_{41} \end{bmatrix}$$

From (18), we obtain the oscillation angle equation:

$$\ddot{q}_2 = -M_{22}^{-1}[M_{21}\ddot{q}_1 + C_{21}\dot{q}_1 + C_{22}\dot{q}_2 + G_2] \tag{19}$$

Substituting (19) into (17):

$$\begin{aligned}&\left[M_{11}-M_{12}M_{22}^{-1}M_{21}\right]\ddot{q}_1+\left[C_{11}-M_{12}M_{22}^{-1}C_{21}\right]\dot{q}_1\\&+\left[C_{12}-M_{12}M_{22}^{-1}C_{22}\right]\dot{q}_2-M_{12}M_{22}^{-1}G_2=u\end{aligned}\tag{20}$$

Let $A_1=M_{11}-M_{12}M_{22}^{-1}M_{21}, B_1=C_{11}-M_{12}M_{22}^{-1}C_{21}$, $D_1=C_{12}-M_{12}M_{22}^{-1}C_{22}, E_1=-M_{12}M_{22}^{-1}G_2$, the system can be compactly written as:

$$A_1\ddot{q}_1+B_1\dot{q}_1+D_1\dot{q}_2+E_1=u\tag{21}$$

Define $q_{1d}=[\theta_{rd},\theta_{ld}]^T$ is the reference wheel angle vector, the wheel angle error signal is calculated as:

$$e=q_1-q_{1d}.\tag{22}$$

Thus, the model can be represented in the error form as:

$$A_1\ddot{e}+B_1\dot{e}+F_d=u\tag{23}$$

where $F_d=A_1\ddot{q}_{1d}+B_1\dot{q}_{1d}+D_1\dot{q}_2+E_1$

By introducing a positive diagonal matrix $\Lambda\in R^{2\times2}$, the expression can be reformulated as:

$$u=\Lambda\ddot{e}+\Lambda\dot{e}+P_d\tag{24}$$

where $\Lambda=\begin{bmatrix}\Lambda_1&0\\0&\Lambda_2\end{bmatrix}$, and
$P_d=(B_1-\Lambda)\dot{e}+(A_1-\Lambda)\ddot{e}+A_1\ddot{q}_{1d}+B_1\dot{q}_{1d}+D_1\dot{q}_2+E_1$.

The sliding surface S is chosen as:

$$S=e+\lambda\dot{e}\tag{25}$$

where $\lambda\in\mathbb{R}^{2\times2}$ denotes a positive definite sliding surface slope matrix. The proposed PD-SMC controller is designed as [20]:

$$u=-K_pe-K_d\dot{e}+K_\theta(\dot{\theta}_1^2+\dot{\theta}_2^2)\dot{e}-K_s\tanh(S)\tag{26}$$

where $K_p,K_d,K_s,K_\theta\in R^{2\times2}$ are positive definite diagonal matrices. In (26), $u_{pd}=-K_pe-K_d\dot{e}$ represents the PD component, $u_{SMC}=-K_s\tanh(S)$ denotes the SMC component. In contrast to conventional PD-SMC controllers, in the proposed control algorithm, $u_{swing}=-K_\theta(\dot{\theta}_1+\dot{\theta}_2)^2e$ is added for the swing suppression.

3.2. Stability analysis

To prove the system stability, the following assumptions are given.

Assumption 1: There exists a positive constant such that:

$$|\dot{\theta}_1\ddot{\theta}_1+\dot{\theta}_2\ddot{\theta}_2|<\sigma\tag{27}$$

Assumption 2: The swing angles of the payload satisfy:

$$-\frac{\pi}{2}<\theta_1<\frac{\pi}{2},\quad -\frac{\pi}{2}<\theta_2<\frac{\pi}{2}\tag{28}$$

Assumption 3: P_d is bounded: $\|P_d\|<+\infty$.

With these assumptions, We will show that the proposed PD–SMC control law described in (26) can drive the system to the desired position and suppress the payload oscillations:

$$\begin{aligned}&\lim_{t\to\infty}\begin{bmatrix}\theta_r&\theta_l&\dot{\theta}_r&\dot{\theta}_l&\theta_1&\theta_2&\dot{\theta}_1&\dot{\theta}_2\end{bmatrix}^T\\&=\begin{bmatrix}\theta_{rd}&\theta_{ld}&0&0&0&0&0&0\end{bmatrix}^T\end{aligned}\tag{29}$$

if the following conditions are satisfied:

$$\begin{cases}K_p>\sigma K_\theta\\K_d>\lambda^{-1}\Lambda\\K_s>||P_d||\end{cases}\tag{30}$$

To establish the stability of the proposed PD-SMC scheme, it suffices to demonstrate that the matrix W given below is positive definite:

$$W=\begin{bmatrix}K_d&\Lambda\\\Lambda&\lambda\Lambda\end{bmatrix}\tag{31}$$

The Lyapunov function is defined by:

$$\begin{aligned}V_{all}(t)=&\frac{1}{2}\begin{bmatrix}e^T&\dot{e}^T\end{bmatrix}W\begin{bmatrix}e\\\dot{e}\end{bmatrix}\\&+\frac{1}{2}\lambda e^TK_pe+\frac{1}{2}K_\theta(\dot{\theta}_1^2+\dot{\theta}_2^2)e^Te+\frac{1}{2}e^T\Lambda e\end{aligned}\tag{32}$$

According to Schur [21] [22], an arbitrary matrix $Q=\begin{bmatrix}A&B\\B^T&C\end{bmatrix}$ is positive definite if:

$$\begin{cases}A>0\\S=C-B^TA^{-1}B>0\end{cases}\tag{33}$$

Applying this to the matrix W and using condition (30):

$$\begin{cases}K_d>0\\S=\lambda\Lambda-\Lambda^TK_d^{-1}\Lambda>0\end{cases}\implies W>0.\tag{34}$$

Thus, the Lyapunov candidate function satisfies $V_{all}(t)\geq0$. The derivative of the Lyapunov candidate function can be expressed as:

$$\begin{aligned}\dot{V}_{all}(t)=&\begin{bmatrix}e^T&\dot{e}^T\end{bmatrix}\begin{bmatrix}K_d&\Lambda\\\Lambda&\lambda\Lambda\end{bmatrix}\begin{bmatrix}\dot{e}\\\ddot{e}\end{bmatrix}+e^T\lambda K_p\dot{e}\\&+e^TK_\theta(\dot{\theta}_1^2+\dot{\theta}_2^2)\dot{e}+e^TK_\theta(\dot{\theta}_1\ddot{\theta}_1+\dot{\theta}_2\ddot{\theta}_2)e+e^T\Lambda\dot{e}\\&=-S^T(K_s\text{sign}(S)+P_d)-e^T\left(K_p-K_\theta(\dot{\theta}_1\ddot{\theta}_1+\dot{\theta}_2\ddot{\theta}_2)\right)e\\&-\dot{e}^T(\lambda K_d-\Lambda)\dot{e}-\dot{e}^T\lambda K_\theta(\dot{\theta}_1^2+\dot{\theta}_2^2)\dot{e}-\dot{e}^T\lambda\Lambda\dot{e}\end{aligned}\tag{35}$$

To ensure the reachability condition and the stability of the sliding surface, let us consider the following inequalities:

$$S^TK_s\,\text{sign}(S)\geq\|S\|K_s\rightarrow-S^TK_s\,\text{sign}(S)\leq-\|S\|K_s\tag{36}$$

$$-S^TP_d\leq|S^TP_d|\leq\|S\|\|P_d\|\tag{37}$$

By summing these two inequalities, from (30), we obtain:

$$-S^T(K_s\,\text{sign}(S)+P_d)\leq-\|S\|(K_s-\|P_d\|)\leq0\tag{38}$$

From (27), (30) and (38), (35) can be rewritten:

$$\begin{aligned}\dot{V}_{all}\leq&-\|S\|(K_s-\|P_d\|)-e^T(K_p-K_\theta\sigma)e\\&-\dot{e}^T(\lambda K_d-\Lambda)\dot{e}-\dot{e}^T\lambda K_\theta(\dot{\theta}_1^2+\dot{\theta}_2^2)\dot{e}-\dot{e}^T\lambda\Lambda\dot{e}\leq0\end{aligned}\tag{39}$$

It can be seen that $\dot{V}_{all}(t)\leq0$. The equality $\dot{V}_{all}(t)=0$ holds if and only if $e=0$ and $\dot{e}=0$. Since the candidate Lyapunov function $V_{all}(t)$ is positive definite and $\dot{V}_{all}(t)$is negative definite, the patient lifting and transferring system controlled by the

designed PD-SMC controller is asymptotically stable. When the system states reach the sliding manifold, both the tracking error and its derivative converge asymptotically to zero, in the sense that:

$$\lim_{t\to\infty} e = 0, \quad \lim_{t\to\infty} \dot{e} = 0, \quad \lim_{t\to\infty} q_1 = q_{1d}, \quad \lim_{t\to\infty} \dot{q}_1 = 0 \tag{40}$$

Therefore, it can be readily concluded that:

$$\lim_{t\to\infty} S = 0, \quad \lim_{t\to\infty} u = 0 \tag{41}$$

Inserting (40) into (16) ,it is derived that:

$$\begin{aligned}&(-p_5 s_1 s_2 + p_8 c_1 + p_9 s_2)\ddot{\theta}_1 + (p_5 c_1 c_2 + p_9 c_1 s_1 c_2)\ddot{\theta}_2 \\ &- p_5 c_1 s_2(\dot{\theta}_1^2 + \dot{\theta}_2^2) - 2p_5 s_1 c_2 \dot{\theta}_1 \dot{\theta}_2 \\ &- p_8 s_1 \dot{\theta}_1^2 + 2p_9 c_2 c_1^2 \dot{\theta}_1 \dot{\theta}_2 - p_9 c_1 s_1 s_2 \dot{\theta}_2^2 = 0\end{aligned} \tag{42}$$

$$\begin{aligned}&(-p_5 s_1 s_2 - p_8 c_1 - p_9 s_2)\ddot{\theta}_1 + (p_5 c_1 c_2 - p_9 c_1 s_1 c_2)\ddot{\theta}_2 \\ &- p_5 c_1 s_2(\dot{\theta}_1^2 + \dot{\theta}_2^2) - 2p_5 s_1 c_2 \dot{\theta}_1 \dot{\theta}_2 \\ &+ p_8 s_1 \dot{\theta}_1^2 - 2p_9 c_2 c_1^2 \dot{\theta}_1 \dot{\theta}_2 + p_9 c_1 s_1 s_2 \dot{\theta}_2^2 = 0\end{aligned} \tag{43}$$

$$\begin{aligned}&p_6 \ddot{\theta}_1 + p_6 c_1 s_1 \dot{\theta}_2^2 + m_d g L_d s_1 c_2 = 0 \\ &\rightarrow \ddot{\boldsymbol{\theta}}_{\mathbf{1}} = -c_1 s_1 \dot{\theta}_2^2 - \frac{m_d g L_d s_1 c_2}{p_6}\end{aligned} \tag{44}$$

$$\begin{aligned}&p_6 c_1^2 \ddot{\theta}_2 - 2p_6 s_1 c_1 \dot{\theta}_2 \dot{\theta}_1 + m_d g L_d c_1 s_2 = 0 \\ &\rightarrow \ddot{\boldsymbol{\theta}}_{\mathbf{2}} = \frac{2s_1}{c_1}\dot{\theta}_2 \dot{\theta}_1 - \frac{m_d g L_d s_2}{p_6 c_1}\end{aligned} \tag{45}$$

By adding and subtracting equations (42) and (43), we obtain the following expressions:

$$-s_1 s_2 \ddot{\theta}_1 + c_1 c_2 \ddot{\theta}_2 - c_1 s_2(\dot{\theta}_1^2 + \dot{\theta}_2^2) - 2s_1 c_2 \dot{\theta}_1 \dot{\theta}_2 = 0 \tag{46}$$

$$\begin{aligned}&(p_8 c_1 + p_9 s_2)\ddot{\theta}_1 + p_9 c_1 s_1 c_2 \ddot{\theta}_2 - p_8 s_1 \dot{\theta}_1^2 \\ &+ 2p_9 c_2 c_1^2 \dot{\theta}_1 \dot{\theta}_2 - p_9 c_1 s_1 s_2 \dot{\theta}_2^2 = 0\end{aligned} \tag{47}$$

By substituting equations (44) and (45) into (46) and performing simplification, we get:

$$s_2 \left(\frac{m_d g L_d}{p_6} c_2 c_1^2 + c_1 \dot{\theta}_1^2 + c_1^3 \dot{\theta}_2^2 \right) = 0 \tag{48}$$

As described in Assumption 1, $c_1, c_2 > 0$, the function in the bracket is always positive. As a consequence, we have:

$$s_2 = 0 \rightarrow \theta_2 = 0, \quad \dot{\theta}_2 = 0 \tag{49}$$

Substituting (44), (45), and (49) into (47) and simplifying:

$$p_8 \frac{m_d g L_d}{p_6} c_1 s_1 c_2 + p_8 s_1 \dot{\theta}_1^2 = 0 \tag{50}$$

Again, using $c_1, c_2 > 0$, it is obtained that:

$$s_1 = 0 \rightarrow \theta_1 = 0, \quad \dot{\theta}_1 = 0 \tag{51}$$

After gathering the results of (49), (51), and (40),the stability of the system has been proven.

4. Simulation results

To evaluate the feasibility and performance of the proposed PD-SMC strategy, numerical simulations were conducted utilizing the MATLAB/Simulink software environment. To ensure strict numerical stability and to accurately capture the high-frequency switching dynamics inherent in the sliding mode control law, the simulation was explicitly configured using a fixed-step solver, specifically ode4 (Runge-Kutta), with a fundamental sample time of 0.001 seconds. This high-resolution temporal configuration is crucial for correctly computing the highly nonlinear dynamics of the underactuated Euler-Lagrange model without inducing artificial chattering. The following subsections present the system's responses under various operating scenarios, including variations in payload mass and suspension cable length, to demonstrate the controller's effectiveness in trajectory tracking and swing suppression.

4.1. Straight trajectory

In the first simulation, the vehicle follows a straight trajectory under varying load weights of 40 kg, 60 kg, and 80 kg. Results appear in Figures 5–8. The system accurately tracks the reference trajectory with no horizontal vibration ($\theta_1 \approx 0$ degrees). Longitudinal vibration persists but remains acceptable with a maximum value of $\theta_1 \approx 5.4$ degrees, and decays rapidly after acceleration ends. Notably, maximum vibration decreases as load weight increases.

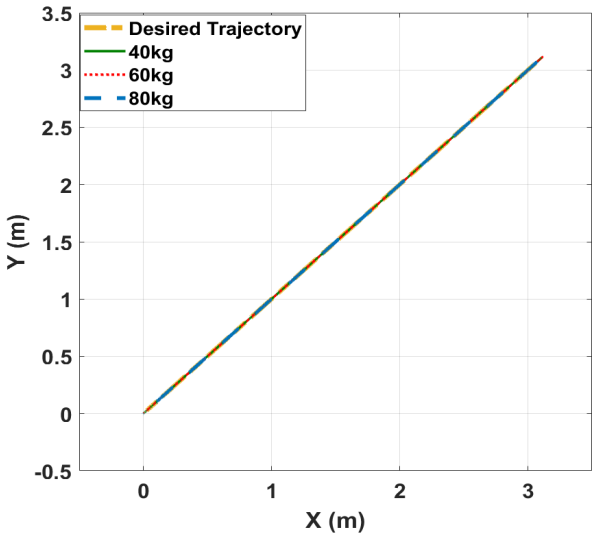

Figure 5: Vehicle trajectory in the straight motion case with varying loads

Simulations with rope length variations of 0.3m, 0.4m, and 0.5m are also done and the results are shown in Figure 9-12. The proposed controller delivers superior tracking, with the vehicle following the reference path via minimal deviation across the full motion. It starts from rest, accelerates smoothly, holds steady velocity, and stops precisely at the target-validating precise, stable control. Swing angle θ_1 is virtually eliminated, while θ_2 damps out quickly showcasing effective vibration suppression and oscillation damping. Oscillation amplitudes stay low (≈ 6 degrees), preventing residual buildup. Control signals remain bounded and smooth, well within actuator limits

for safe operation. Overall, this strategy ensures high trajectory accuracy, robust vibration suppression, and reliable payload handling under simple conditions, paving the way for complex maneuvers.

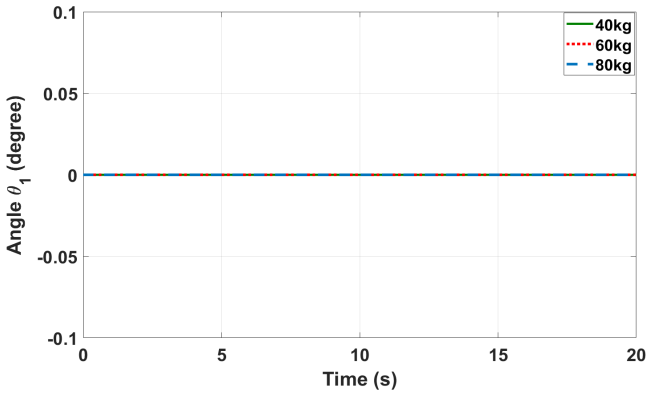

Figure 6: Swing angle θ_1 in the straight motion case with varying loads

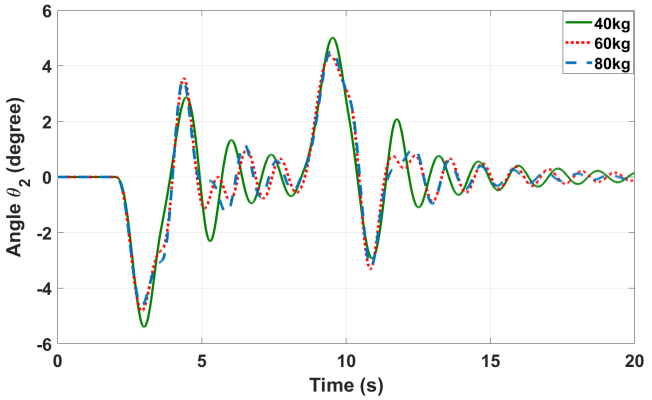

Figure 7: Swing angle θ_2 in the straight motion case with varying loads

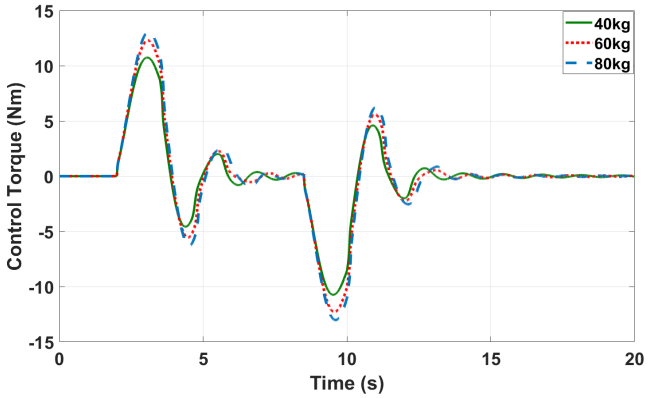

Figure 8: Control torque in the straight motion case with varying loads

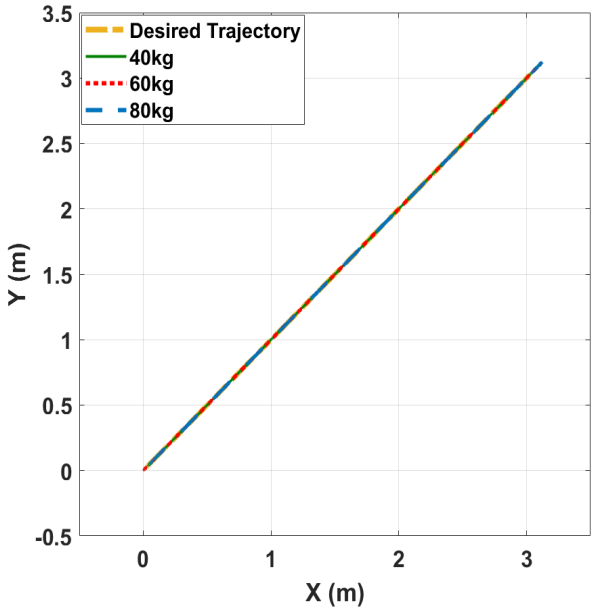

Figure 9: Vehicle trajectory in the straight motion case with varying rope lengths

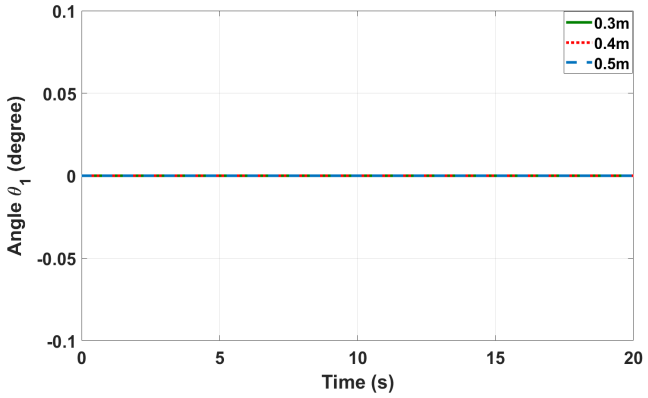

Figure 10: Swing angle θ_1 in the straight motion case with varying rope lengths

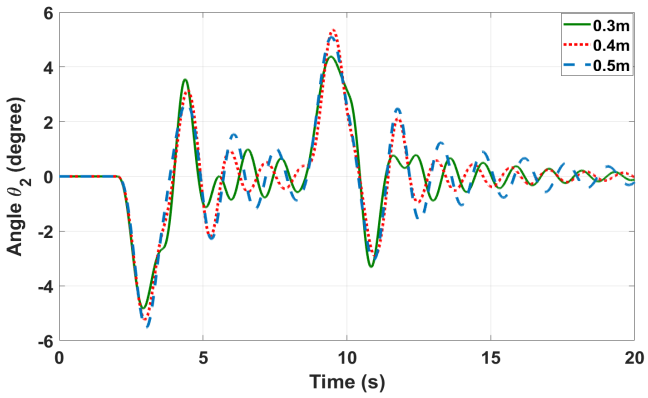

Figure 11: Swing angle θ_2 in the straight motion case with varying rope lengths

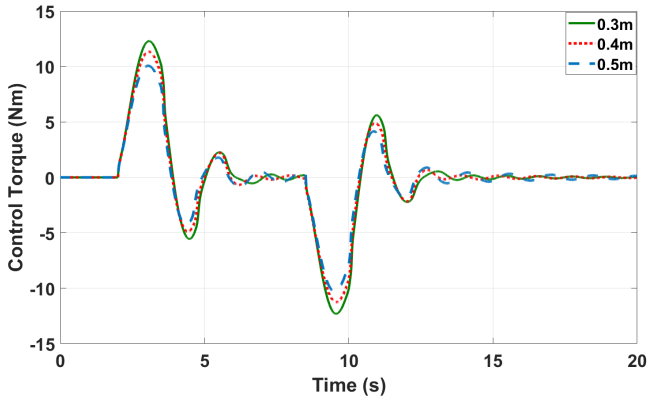

Figure 12: Control torque in the straight motion case with varying rope lengths

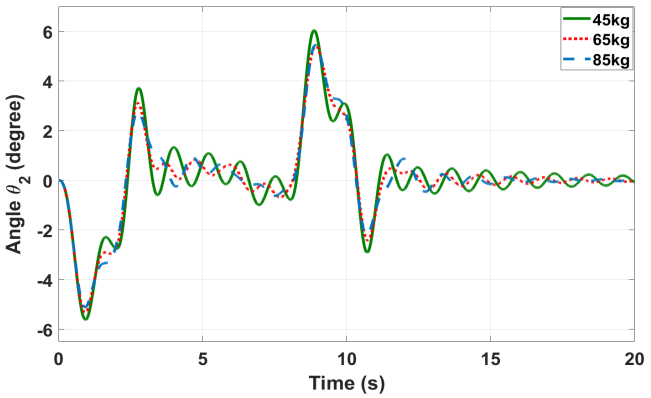

Figure 15: Swing angle θ_2 in the curved motion case with varyingloads

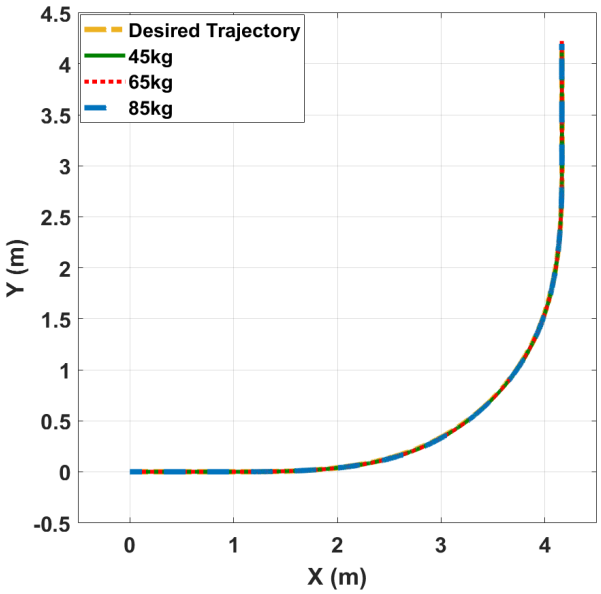

Figure 13: Vehicle trajectory in the curved motion case with varying loads

4.2. Curved trajectory

In this scenario, the vehicle moves straight, turns into a corridor, and resumes straight motion. Simulations test varying load weights (45 kg, 65 kg, 85 kg) and rope lengths (0.25 m, 0.35 m, 0.45 m). The simulation results are shown in Figures 13-16 for varying load weight, and in Figures 20-19 for varying rope length.

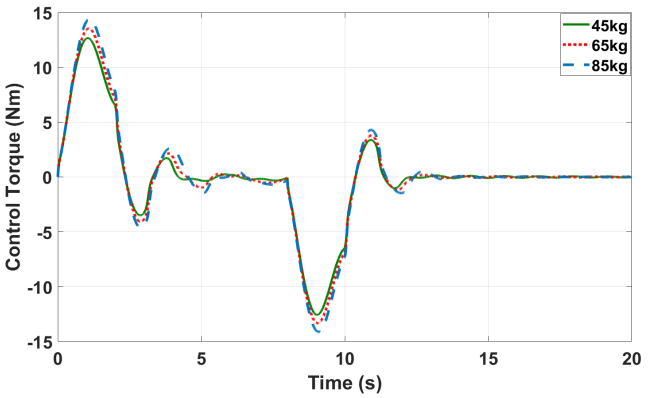

Figure 16: Control torque in the curved motion case with varying loads

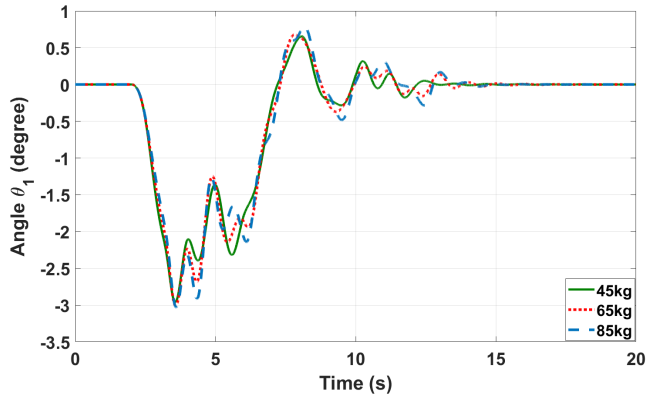

Figure 14: Swing angle θ_1 in the curved motion case with varying loads

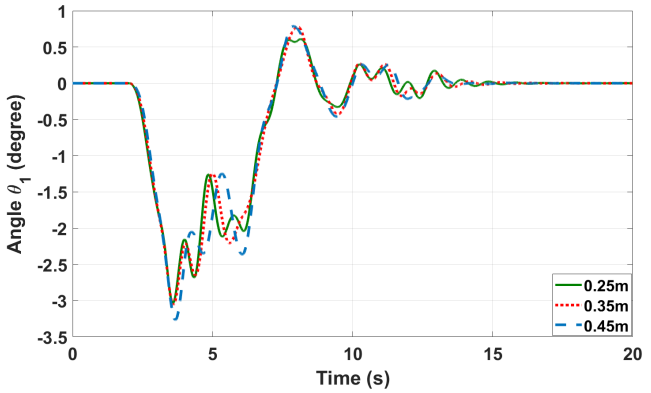

Figure 17: Swing angle θ_1 in the curved motion case with varying rope lengths

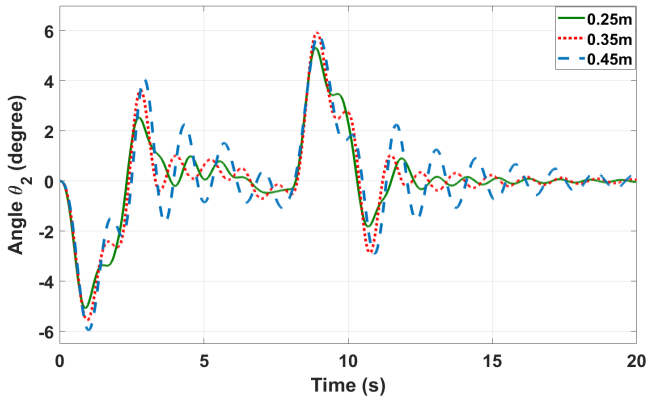

Figure 18: Swing angle θ_2 in the curved motion case with varying rope lengths

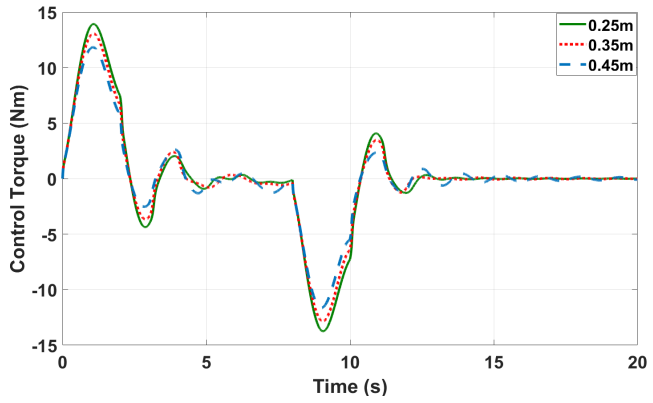

Figure 19: Control torque in the curved motion case with varying rope lengths

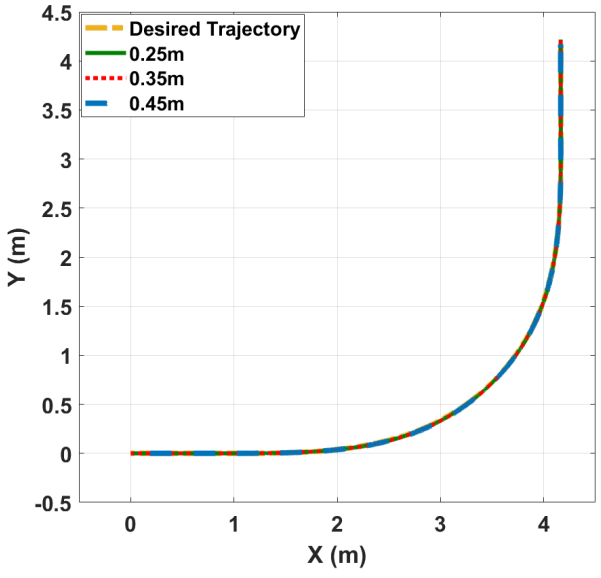

Figure 20: Vehicle trajectory in the curved motion case with varying rope lengths

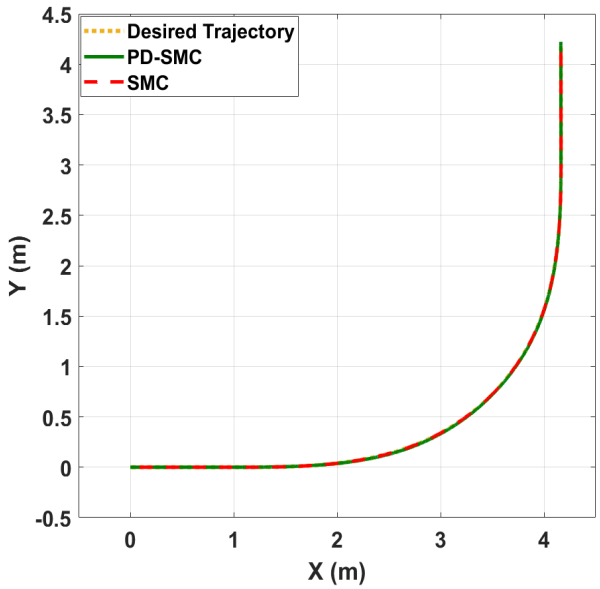

Figure 21: Comparison of trajectory tracking in the curved motion case

5. Comparison of controllers

To rigorously evaluate the effectiveness and superiority of the proposed approach, this section presents a comparative analysis between the PD-SMC and a standard Sliding Mode Controller (SMC). The performance of both controllers is assessed based on three primary criteria: motion trajectory tracking accuracy, the ability to suppress payload oscillations, and the smoothness of the generated control signals. To ensure a fair and objective comparison, the simulation scenarios for both controllers are conducted under identical operating conditions, system parameters, and external disturbances. The comparative results are detailed below.

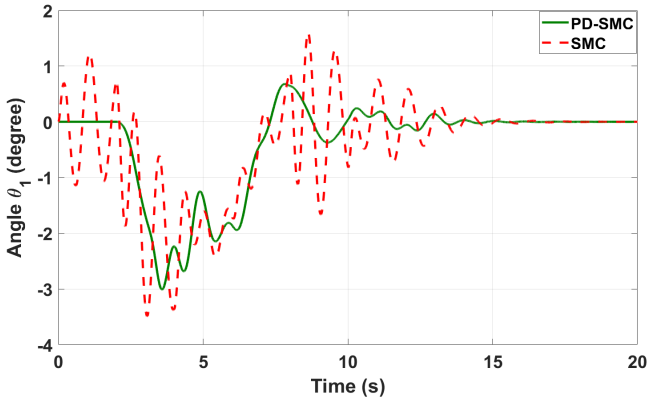

Figure 22: Comparison of swing angle θ_1 in the curved motion case

The simulation results (Figures 21–28) demonstrate that while both the proposed PD-SMC and the standard SMC achieve excellent trajectory tracking accuracy, the PD-SMC is significantly superior in sway suppression and control effort generation. Unlike the standard SMC, which exhibits high-frequency payload oscillations and severe control torque chattering, the PD-SMC effectively dampens the swing angles, forcing them to converge smoothly and rapidly to zero. Furthermore, the linear action of the PD component enables the PD-SMC to generate a smooth, continuous, and bounded con-

trol signal, thereby eliminating abrupt mechanical shocks and ensuring safe, stable operation for the physical actuators.

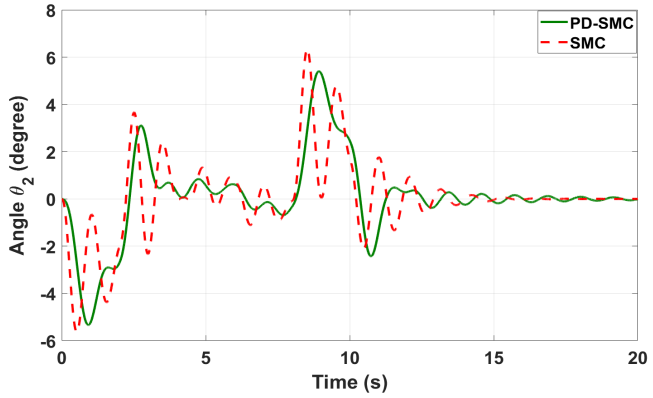

Figure 23: Comparison of swing angle θ_2 in the curved motion case

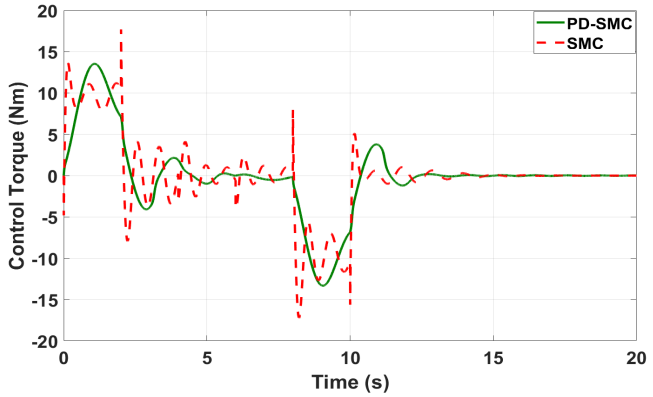

Figure 24: Comparison of control torque in the curved motion case

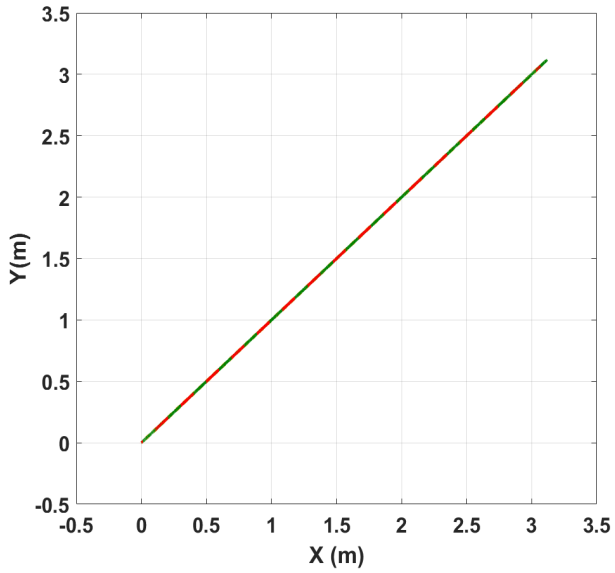

Figure 25: Comparison of trajectory tracking in the straight motion case

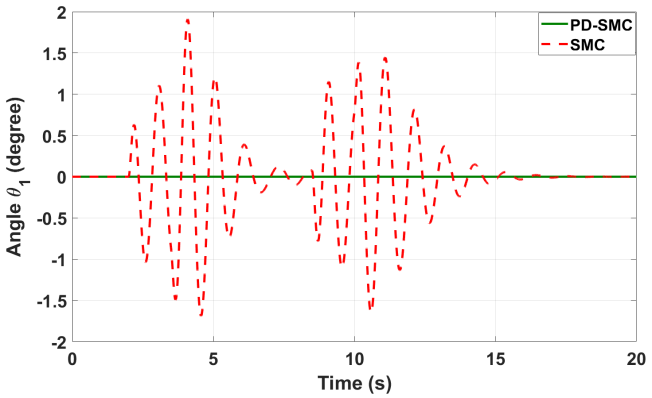

Figure 26: Comparison of swing angle θ_1 in the straight motion case

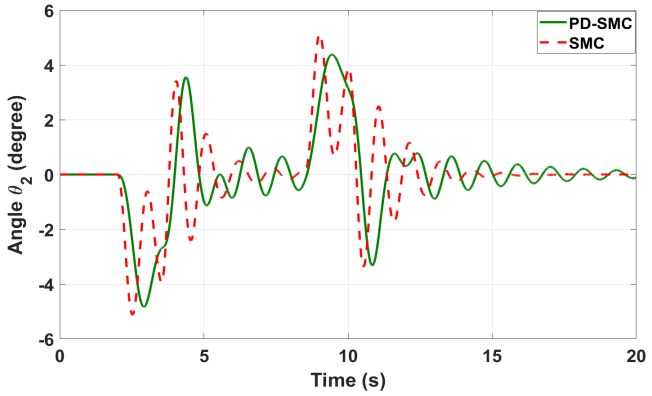

Figure 27: Comparison of swing angle θ_2 in the straight motion case

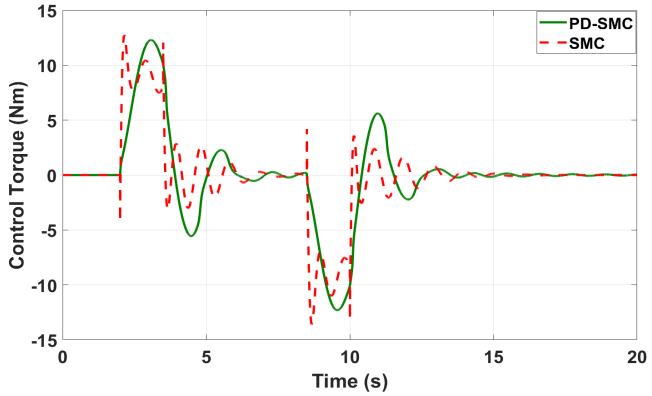

Figure 28: Comparison of control torque in the straight motion case

6. Conclusions

This paper introduces a PD-SMC controller for a patient lifting and transferring support system. It combines the straightforward, easy-to-implement PD control with a sliding surface for robust feedback, ensuring absolute stability despite external disturbances and model uncertainties. By defining the sliding surface from state errors, the design eliminates the chattering typical of traditional SMC while keeping trajectory tracking errors minimal. Simulations demonstrate the controller's superiority through rapid response, precise positioning, and effective load oscillation suppression-maintaining top performance amid payload changes or varying cable lengths.

A. Appendix A: System model components

System model

$$M(q)\ddot{q}+C(q,\dot{q})\dot{q}+G(q)=\tau$$

where,

$$\mathbf{M}=\begin{bmatrix} m_{11} & m_{12} & m_{13} & m_{14} \\ m_{21} & m_{22} & m_{23} & m_{24} \\ m_{31} & m_{32} & m_{33} & m_{34} \\ m_{41} & m_{42} & m_{43} & m_{44} \end{bmatrix}, \mathbf{C}=\begin{bmatrix} c_{11} & c_{12} & c_{13} & c_{14} \\ c_{21} & c_{22} & c_{23} & c_{24} \\ c_{31} & c_{32} & c_{33} & c_{34} \\ c_{41} & c_{42} & c_{43} & c_{44} \end{bmatrix}$$

$$\mathbf{G}=\begin{bmatrix} 0 \\ 0 \\ g_{31} \\ g_{41} \end{bmatrix}, \quad \tau=\begin{bmatrix} \tau_r \\ \tau_l \\ 0 \\ 0 \end{bmatrix} \text{ and,}$$

$$p_1=\frac{m_p r^2}{4}+\frac{I_p r^2}{d^2}+I_{yw}+\frac{2I_{zw}r^2}{d^2}+m_w r^2+\frac{m_d r^2}{4}$$
$$+\frac{m_d L_2^2 r^2}{d^2}+\frac{I_d r^2}{d^2}$$

$$p_2=\frac{m_p r^2}{4}+\frac{I_p r^2}{d^2}-\frac{2I_{zw}r^2}{d^2}-\frac{m_d r^2}{2}-\frac{2m_d L_2^2 r^2}{d^2}-\frac{I_d r^2}{d^2}$$

$$p_3=m_d L_d^2\frac{r^2}{d^2}, \quad p_4=\frac{2m_d L_d L_2 r^2}{d^2}, \quad p_5=\frac{1}{2}m_d r L_d,$$

$$p_6=m_d L_d^2, \quad p_7=\frac{m_d L_d^2 r}{d},$$

$$p_8=\frac{m_d L_d L_2 r}{d}, \quad p_9=\frac{m_d L_d^2 r}{d}$$

$$c_1=\cos\theta_1, \quad s_1=\sin\theta_1$$

$$c_2=\cos\theta_2, \quad s_2=\sin\theta_2$$

$$m_{11}=p_1+p_3(c_1^2s_2^2+s_1^2)+p_4c_1s_2-p_7s_1$$

$$m_{12}=m_{21}=p_2-p_3(c_1^2s_2^2+s_1^2)-p_4c_1s_2$$

$$m_{13}=m_{31}=-p_5s_1s_2+p_8c_1+p_9s_2$$

$$m_{14}=m_{41}=p_5c_1c_2+p_9c_1s_1c_2$$

$$m_{22}=p_1+p_3(c_1^2s_2^2+s_1^2)+p_4c_1s_2+p_7s_1$$

$$m_{23}=m_{32}=-p_5s_1s_2-p_8c_1-p_9s_2$$

$$m_{24}=m_{42}=p_5c_1c_2-p_9c_1s_1c_2$$

$$m_{33}=p_6$$

$$m_{34}=m_{43}=0$$

$$m_{44}=p_6c_1^2$$

$$c_{11}=p_3(c_1s_1c_2^2\dot{\theta}_1+c_1^2c_2s_2\dot{\theta}_2)$$
$$+\frac{p_4}{2}(-s_1s_2\dot{\theta}_1+c_1c_2\dot{\theta}_2)-\frac{p_7}{2}c_1\dot{\theta}_1$$

$$c_{12}=-p_3(c_1s_1c_2^2\dot{\theta}_1+c_1^2c_2s_2\dot{\theta}_2)$$
$$+\frac{p_4}{2}(s_1s_2\dot{\theta}_1-c_1c_2\dot{\theta}_2)$$

$$c_{13}=p_3c_1s_1c_2^2(\dot{\theta}_r-\dot{\theta}_l)-\frac{p_4}{2}s_1s_2(\dot{\theta}_r-\dot{\theta}_l)$$
$$-p_5(c_1s_2\dot{\theta}_1+s_1c_2\dot{\theta}_2)-\frac{p_7}{2}c_1\dot{\theta}_r-p_8s_1\dot{\theta}_1+p_9c_2^2s_2^2\dot{\theta}_2$$

$$c_{14}=p_3c_1^2c_2s_2(\dot{\theta}_r-\dot{\theta}_l)+\frac{p_4}{2}c_1c_2(\dot{\theta}_r-\dot{\theta}_l)$$
$$-p_5(s_1c_2\dot{\theta}_1+c_1s_2\dot{\theta}_2)+p_9(c_2^2c_1\dot{\theta}_1-c_1s_1s_2\dot{\theta}_2)$$

$$c_{21}=-p_3(c_1s_1c_2^2\dot{\theta}_1+c_1^2c_2s_2\dot{\theta}_2)$$
$$+\frac{p_4}{2}(s_1s_2\dot{\theta}_1-c_1c_2\dot{\theta}_2)$$

$$c_{22}=p_3(c_1s_1c_2^2\dot{\theta}_1+c_1^2c_2s_2\dot{\theta}_2)$$
$$+\frac{p_4}{2}(-s_1s_2\dot{\theta}_1+c_1c_2\dot{\theta}_2)+\frac{p_7}{2}c_1\dot{\theta}_1$$

$$c_{23}=-p_3c_1s_1c_2^2(\dot{\theta}_r-\dot{\theta}_l)+\frac{p_4}{2}s_1s_2(\dot{\theta}_r-\dot{\theta}_l)$$
$$-p_5(c_1s_2\dot{\theta}_1+s_1c_2\dot{\theta}_2)+\frac{p_7}{2}c_1\dot{\theta}_l+p_8s_1\dot{\theta}_1-p_9c_2^2s_2^2\dot{\theta}_2$$

$$c_{24}=-p_3c_1^2c_2s_2(\dot{\theta}_r-\dot{\theta}_l)-\frac{p_4}{2}c_1c_2(\dot{\theta}_r-\dot{\theta}_l)$$
$$-p_5(s_1c_2\dot{\theta}_1+c_1s_2\dot{\theta}_2)-p_9(c_2^2c_1\dot{\theta}_1-c_1s_1s_2\dot{\theta}_2)$$

$$c_{31}=-p_3c_1s_1c_2^2(\dot{\theta}_r-\dot{\theta}_l)+\frac{p_4}{2}s_1s_2(\dot{\theta}_r-\dot{\theta}_l)$$
$$+\frac{p_7}{2}c_1\dot{\theta}_r+p_9c_2^2s_2^2\dot{\theta}_2$$

$$c_{32}=p_3c_1s_1c_2^2(\dot{\theta}_r-\dot{\theta}_l)-\frac{p_4}{2}s_1s_2(\dot{\theta}_r-\dot{\theta}_l)$$
$$-\frac{p_7}{2}c_1\dot{\theta}_l-p_9c_2^2s_1^2\dot{\theta}_2$$

$$c_{33}=0$$

$$c_{34}=p_9c_2^2s_1^2(\dot{\theta}_r-\dot{\theta}_l)+p_6c_1s_1\dot{\theta}_2$$

$$c_{41}=-p_3c_1^2c_2s_2(\dot{\theta}_r-\dot{\theta}_l)-\frac{p_4}{2}c_1c_2(\dot{\theta}_r-\dot{\theta}_l)-p_9c_2s_1^2\dot{\theta}_1$$

$$c_{42}=p_3c_1^2c_2s_2(\dot{\theta}_r-\dot{\theta}_l)+\frac{p_4}{2}c_1c_2(\dot{\theta}_r-\dot{\theta}_l)+p_9c_2s_1^2\dot{\theta}_1$$

$$c_{43}=-p_6s_1c_1\dot{\theta}_2-p_9c_2s_1^2(\dot{\theta}_r-\dot{\theta}_l)$$

$$c_{44}=-p_6s_1c_1\dot{\theta}_1$$

$$g_{31}=m_dgL_d\sin\theta_1\cos\theta_2$$

$$g_{41}=m_dgL_d\cos\theta_1\sin\theta_2$$

References

[1] S. Hellmers, A. Brinkmann, C. Fifelski-von Böhlen, S. Lau, R. Diekmann, and A. Hein, “Posture and mechanical load assessment during patient transfers,” SN Computer Science, vol. 3, no. 5, article no. 375, Jul. 2022, doi: 10.1007/s42979-022-01263-1.

[2] Mobile patient lift - https://www.hillrom.cn/en/products/sph-mobile-lifts.

[3] Patient lift - https://vivamobilityusa.com/products/handicare-c450-fixed ceiling-lift.

[4] Wall Lift System, https://www.surehands.com/products/wall-lift-system.

[5] D. Callon, I. Lalonde, M. Nadeau, and A. Girard, “Controller design and experimental evaluation of a motorised assistance for a patient transfer floor lift,” arXiv preprint arXiv:2205.15201, 2022. [Online]. Available: https://arxiv.org/abs/2205.15201.

[6] R. Ranasinghe, L. Dantanarayana, A. Tran, S. Lie, M. Behrens and L. Liu, "Smart hoist: An assistive robot to aid carers," 2014 13th International Conference on Control Automation Robotics & Vision (ICARCV), Singapore, 2014, pp. 1285-1291, doi: 10.1109/IC.

[7] A. Althomali, M. Almalki, M. Alotaibi, A. Alshahrani và S. Almutairi, “Strategies to Improve Safe Patient Handling and Mobility Programs: A Systematic Review,” International Journal of Environmental Research and Public Health, vol. 21, no. 1, Article 1659, 2024, doi: 10.3390/ijerph210101659.

[8] Z. Y. Nie, et al., “Design, analysis and application of a new disturbance rejection scheme for PID control,” ISA Transactions, vol. 99, pp. 310–324, 2020.

[9] T. L. Tong, V. T. Duong, T. P. Tran and M. D. Duong, "Enhancing Sliding Mode Control for a Mobile Patient Lifting Device," 2025 International Conference on Advanced Technologies for Communications (ATC), Hanoi, Vietnam, 2025, pp. 1-6, doi: 10.1109/ATC6761.

[10] T. L. Tong, T. A. Nguyen, and M. D. Duong, “Flatness-Based Linear Active Disturbance Rejection Control for Tower Crane,” FME Transactions, vol. 53, no. 2, pp. 270–279, 2025.

[11] G. Herbst, "A Simulative Study on Active Disturbance Rejection Control (ADRC) as a Control Tool for Practitioners," 2013.

[12] G. Chen, “Vibration Suppression in a Two-Mass Drive System Using Three Input Shaping – Comparative Study,” in Proceedings of the IEEE International Conference on Consumer Electronics & Computer Engineering (ICCECE), 2023, pp. 68–73, doi: 10.1109/ICC ECE59400.10238602.

[13] L. Ramli, Z. Mohamed, and H. I. Jaafar, "A neural network-based input shaping for swing suppression of an overhead crane under payload hoisting and mass variations," Mechanical Systems and Signal Processing, vol. 107, pp. 484-501, Jul. 2018, doi: 10.1016/j.ymssp.2018.01.029.
[14] K. J. Kim, J. B. Park, and Y. H. Choi, "Chattering Free Sliding Mode Control," in Proceedings of the SICE-ICASE International Joint Conference, Busan, Korea, Nov. 2006, pp. 3152–3157, doi: 10.1109/SICE.2006.315237.
[15] M. D. Duong, Q. T. Dao, & T. H. Do, "Settling Time Optimization of a Critically Damped System with Input Shaping for Vibration Suppression Control," Engineering, Technology & Applied Science Research, vol. 12, no. 5, pp. 9388–9394, Oct. 2022, doi: 10.48084/etasr.5242.
[16] Zhang, M. & Jing, X. (2022). Model-Free Saturated PD-SMC Method for 4-DOF Tower Crane Systems. IEEE Transactions on Industrial Electronics, 69(10), 10270–10280.
[17] M. Zhang, Y. Zhang, and X. Cheng, "An Enhanced Coupling PD with Sliding Mode Control Method for Underactuated Double-pendulum Overhead Crane Systems," IEEE Access, vol. 7, pp. 102523–102534, 2019. doi: 10.1109/ACCESS.2019.2929560.
[18] Li, Z.; Ge, S.S. *Fundamentals in Modeling and Control of Mobile Manipulators*; CRC Press: Boca Raton, FL, USA, 2013.
[19] Tzafestas, S.G. *Introduction to Mobile Robot Control*, 2nd ed.; National Technical University of Athens: Athens, Greece, 2014.
[20] M. Zhang, Y. Zhang, H. Chen and X. Cheng, "Model-independent PD-SMC method with payload swing suppression for 3D overhead crane systems," Mech. Syst. Signal Process., vol. 129, pp. 381–393, 2019. doi: 10.1016/j.ymssp.2019.04.046.
[21] P. Ouyang, J. Acob, & V. Pano, "PD with sliding mode control for trajectory tracking of robotic system," Robotics and Computer-Integrated Manufacturing, vol. 30, no. 2, pp. 189–200, Apr. 2014, doi: 10.1016/j.rcim.2013.09.008.
[22] W. Yue, V. Pano, P. Ouyang, & Y. Hu, "Model-independent position domain sliding mode control for contour tracking of robotic manipulator," International Journal of Systems Science, vol. 48, no. 1, pp. 190–199, Jan. 2017, doi: 10.1080/00207721.2016.1183182.